

Evolution of the Spin Hall Magnetoresistance in Cr₂O₃/Pt bilayers close to the Néel temperature

Richard Schlitz,^{1,2, a)} Tobias Kosub,³ Andy Thomas,^{4,2} Savio Fabretti,^{1,2} Kornelius Nielsch,^{4,5} Denys Makarov,³ and Sebastian T. B. Goennenwein^{1,2}

¹⁾*Institut für Festkörper- und Materialphysik, Technische Universität Dresden, 01062 Dresden, Germany*

²⁾*Center for Transport and Devices of Emergent Materials, Technische Universität Dresden, 01062 Dresden, Germany*

³⁾*Helmholtz-Zentrum Dresden-Rossendorf e.V., Institute of Ion Beam Physics and Materials Research, 01328 Dresden, Germany*

⁴⁾*Leibniz Institute for Solid State and Materials Research Dresden (IFW Dresden), Institute for Metallic Materials, 01069 Dresden, Germany*

⁵⁾*Technische Universität Dresden, Institute of Materials Science, 01062 Dresden, Germany*

(Dated: 24 November 2021)

We study the evolution of magnetoresistance with temperature in thin film bilayers consisting of platinum and the antiferromagnet Cr₂O₃ with its easy axis out of the plane. We vary the temperature from 20 °C to 60 °C, close to the Néel temperature of Cr₂O₃ of approximately 37 °C. The magnetoresistive response is recorded during rotations of the external magnetic field in three mutually orthogonal planes. A large magnetoresistance having a symmetry consistent with a positive spin Hall magnetoresistance is observed in the paramagnetic phase of the Cr₂O₃, which however vanishes when cooling to below the Néel temperature. Comparing to analogous experiments in a Gd₃Ga₅O₁₂/Pt heterostructure, we conclude that a paramagnetic field induced magnetization in the insulator is not sufficient to explain the observed magnetoresistance. We speculate that the type of magnetic moments at the interface qualitatively impacts the spin angular momentum transfer, with the 3*d* moments of Cr sinking angular momentum much more efficiently as compared to the more localized 4*f* moments of Gd.

The spin Hall magnetoresistance (SMR),^{1–3} arising from the combined action of the spin Hall⁴ and inverse spin Hall effect is a powerful tool to monitor the magnetization direction in a ferrimagnetic insulator (FMI)/normal metal (NM) hybrid structure.^{2,3} Recent publications furthermore established that the SMR also allows to probe the surface magnetization⁵, and to resolve exotic magnetic phases such as spin canting⁶ and helical magnetic order.⁷ In particular, magnetic phase diagrams could be reconstructed from the SMR response⁶, since the SMR is sensitive to the sublattice magnetization orientations.⁸ Last but not least, increasing interest in antiferromagnetic spintronics^{9–12} led to theoretical investigations¹³ and experimental studies of the spin Hall magnetoresistance in antiferromagnetic insulator (AFMI)/NM heterostructures.^{14–17}

In a FMI/NM bilayer, it often is sufficient to consider the (net) magnetization \mathbf{m} in the FMI. The SMR can then be expressed as¹

$$R_{\text{long}} = R_0 - \Delta R m_t^2 = R_0 - \Delta R \sin^2(\angle(\mathbf{m}, \mathbf{t})) \quad (1)$$

where $\Delta R > 0$ denotes the change in resistance arising as a function of the orientation of the magnetization unit vector \mathbf{m} . m_t is the projection of the magnetization on the direction \mathbf{t} perpendicular to the current direction \mathbf{j} as

well as the surface normal \mathbf{n} . \mathbf{j} , \mathbf{t} and \mathbf{n} are an orthonormal set of unit vectors. According to Eq. 1, the fingerprint of the SMR effect thus is a maximum resistance for $\mathbf{m} \parallel \mathbf{j}$ viz. $\mathbf{m} \parallel \mathbf{n}$, and a smaller resistance otherwise. Additionally, since R_{long} is proportional to $\sin^2(\angle(\mathbf{m}, \mathbf{t}))$ the SMR is symmetric upon magnetization reversal.

Interestingly, SMR experiments in AFMI/NM heterostructures point to a more complex behavior.^{14–17} However, most of the experiments performed to date were carried out in the easy plane AFM NiO, where multiple domains with equivalent energy coexist and can exhibit different magnetoresistance responses. Since the magnetic configuration of an easy axis AFM is much simpler, SMR experiments in such materials appear desirable. Cr₂O₃ is a prototypical easy axis AFM, i.e., this material features one uniaxial anisotropy easy axis, and it was recently established for applications in antiferromagnetic spintronics.^{18,19} Furthermore, the Néel temperature $T_N \approx 37$ °C of bulk Cr₂O₃²⁰ is close to room temperature, allowing for magnetotransport experiments across the AFM/paramagnetic phase transition using a simple thermoelectric cooler/heater.

Thus, we have fabricated thin film heterostructures consisting of Cr₂O₃ and platinum, and measured the evolution of their magnetoresistive response across T_N . Interestingly, we observe a clear SMR signal for $T > T_N$, while the magnetoresistive response below T_N is very small. Our experiments thus show that the SMR in AFMI/NM heterostructures can be used to monitor the Néel transition. Moreover, the evolution of the magne-

^{a)}Electronic mail: richard.schlitz@tu-dresden.de

toresistance with external field orientation above the Néel temperature is consistent with Eq. 1, as expected for an SMR signal originating from the field induced paramagnetic polarization of the AFMI layer. This paramagnetic polarization will always follow the external magnetic field, giving rise to a finite positive magnetoresistance as observed in FMI/Pt heterostructures.^{2,21} Since we here rotate the external magnetic field in three mutually orthogonal planes, we can unambiguously identify the signature of the SMR in our AFMI/NM heterostructures.

The samples were prepared as follows: A 250 nm Cr_2O_3 layer was grown onto c-cut Al_2O_3 substrates using reactive evaporation of Cr from a Knudsen cell in 1×10^{-5} mbar molecular oxygen gas. The substrate temperature was set to 700 °C initially and lowered to 500 °C after the growth of the first few monolayers. Directly after growth, the Cr_2O_3 layer was annealed in vacuum at 750 °C. This leads to an easy axis of the antiferromagnetic anisotropy in the out of plane orientation. Subsequently, a 2 – 3 nm platinum film was sputtered in-situ at 100 °C, resulting in the layer sequence schematically depicted in Fig. 1(a). Note that Cr is expected at the Cr_2O_3 /Pt interface in our samples, which is favorable compared to oxygen terminated interfaces due to the magnetoelectric properties of Cr_2O_3 .^{22,23} For further details about the sample structure please refer to our previous work.^{18,19,24} We then patterned the Cr_2O_3 /Pt bilayers into Hall-bars (cf. Fig. 1(b)) using optical lithography and inverse sputtering with Ar-ions. The contacts used for the voltage measurement are separated by $l = 300 \mu\text{m}$. The width of the Hall-bar is $w = 40 \mu\text{m}$. Finally, the samples were glued onto chip carriers, electrically contacted via wedge bonding and mounted into a magnetotransport setup to characterize the magnetoresistive response. The setup features a cylindrical Halbach array²⁵ generating a constant magnetic flux density $\mu_0 H = 1 \text{ T}$ perpendicular to the array's cylindrical axis. We control the sample temperature with a thermoelectric cooler attached to the sample inserts, enabling us to vary the temperature in the range of 20 °C to 60 °C. The measured temperatures are detected in close vicinity of the sample position with a Pt100 resistance thermometer.

To obtain the magnetoresistive response, we drive a current of $I = 180 \mu\text{A}$ along the Hall-bar with a Keithley 2450 sourcemeter. The voltage drop is simultaneously detected by a Keithley 2182 nanovoltmeter. To increase the measurement sensitivity and to remove thermoelectric contributions, we employ a current reversal technique.²⁶ In the magnetotransport experiments, the Halbach array and, thus, the magnetic field is rotated around the cylindrical axis. By mounting the sample in three different sample inserts, we define three orthogonal rotation planes of the magnetic field. For the first two, the magnetic field is rotated around the surface normal \mathbf{n} (Fig. 1(c), ip) and around the direction of current flow \mathbf{j} (Fig. 1(d), oopj), respectively. In the third case, the magnetic field is rotated around the transverse direction

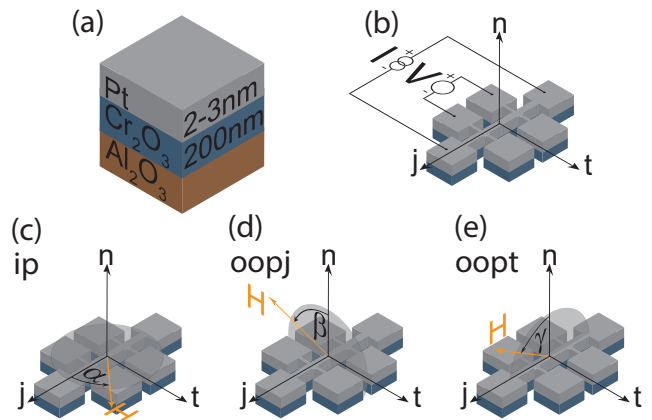


FIG. 1. Panel (a) displays the layer sequence after deposition. The coordinate system spanned by the current direction \mathbf{j} , the surface normal \mathbf{n} and the transverse direction \mathbf{t} as well as the patterned Hall-bar are shown in panel (b). A constant current of $I = 180 \mu\text{A}$ is applied along the Hall-bar and the voltage drop is simultaneously recorded in a four point measurement scheme. The definitions of the three mutually orthogonal magnetic field rotation planes with their angles α , β and γ are depicted in panels (c), (d) and (e), respectively.

to get a complete set of (orthogonal) rotation planes.

The obtained magnetoresistance

$$\frac{R(\alpha, \beta, \gamma)}{\min(R)} - 1$$

of the Cr_2O_3 /Pt sample is shown in Fig. 2 for three different temperatures. The data is corrected to remove linear drifts. Here, the minimum resistance is $\min(R) = 526.5 \Omega$, 539.8Ω and 547.5Ω for $T = 21.6 \text{ °C}$, 37.6 °C and 47 °C for the in-plane data, respectively.

We start the discussion with the data obtained during the ip and oopj rotation of the magnetic field (cf. Fig. 2(a,b, black squares)). Here, a $\sin^2(\alpha)$ modulation is evident at $T = 47 \text{ °C} > T_N$. When the temperature is approaching T_N , the amplitude of the resistance modulation decreases. For $T = 20 \text{ °C}$, the resistance modulation as a function of magnetic field orientation vanishes within our experimental resolution, as one naively would expect considering that the external magnetic field does not affect the AFM spin structure. Below this temperature range, condensation of ambient moisture jeopardizes reliable data taking in the setup used here.

It is important to note that a small $\sin^2(\gamma)$ modulation is also observed for the oopt rotation, leading to the conclusion that in addition to a strong SMR, another effect is present in our structures. It could be attributed to a magnetic proximity effect, as suggested by the field invariant anomalous Hall contribution evident in our as well as similar samples.^{18,19} However, the finite resistance modulation in the oopt rotation could also reflect the crystallinity of the Pt film, giving rise to additional terms in the resistivity tensor due to symmetry as already observed for the anisotropic magnetoresistance.²⁷

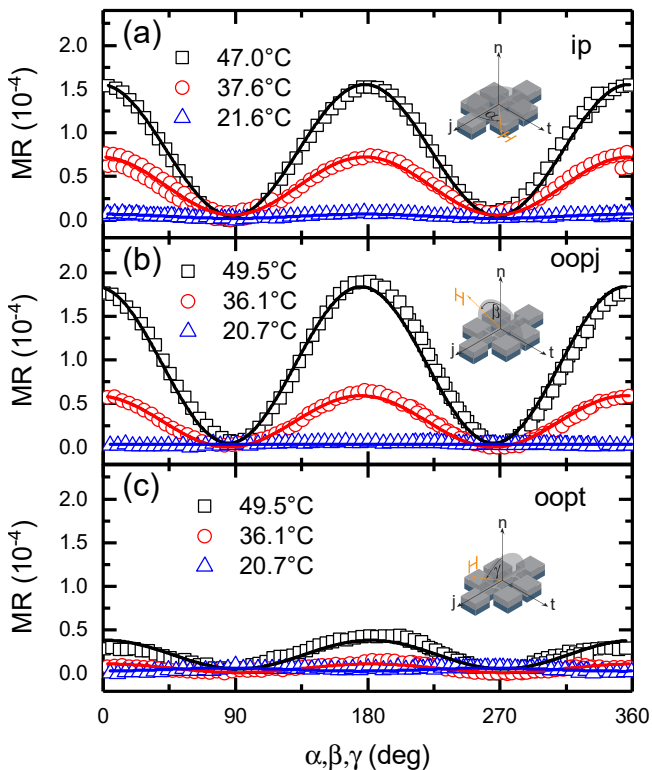


FIG. 2. The magnetoresistance obtained during rotations of the magnetic flux density $\mu_0 H = 1$ T in ip, oopj and oopt configuration for three temperatures are shown in (a), (b) and (c), respectively. The black squares correspond to measurements above the Néel temperature. The data represented by the red circles were measured close to the Néel temperature, while the data shown as blue triangles were recorded just below. $\sin^2(\alpha, \beta, \gamma)$ fits, shown as lines, were performed to extract the amplitude of the signals. A linear slope was subtracted to remove drifts.

By fitting a $\sin^2(\alpha, \beta, \gamma)$ to the data, we can extract the relative magnetoresistance amplitudes for all temperatures and rotation geometries. The obtained results are summarized in Fig. 3. To determine the exact Néel temperature in our heterostructures, we carried out zero-offset anomalous Hall magnetometry measurements.¹⁸ The resulting R_{inv} for positive and negative cooling field is shown in the upper panel of Fig. 3 as black and red symbols, respectively, and yields a Néel temperature of $T_N = 37^\circ\text{C}$ as indicated by the dashed orange line. This is in excellent agreement with the bulk Cr_2O_3 Néel temperature²⁰ of $T_N = 37^\circ\text{C}$, and matches the temperature region where the SMR response changes. The SMR thus reflects the change in antiferromagnetic to paramagnetic order in the insulator. Interestingly, the change in SMR appears to be smeared out in a much broader temperature range as compared to the zero-offset anomalous Hall magnetometry data.

This suggests that the SMR probes a different subset of magnetic moments, since the SMR increases further with increasing temperature even in the paramagnetic

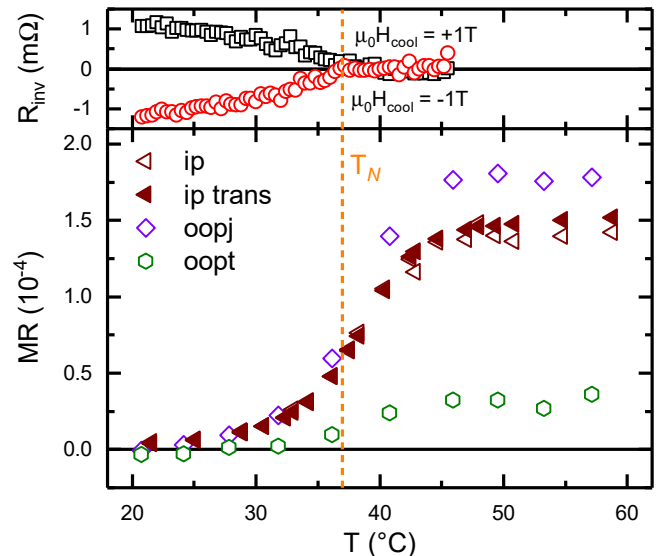


FIG. 3. The upper panel shows the magnetic field invariant contribution R_{inv} to the Hall resistivity acquired by zero-offset anomalous Hall magnetometry for positive (black symbols) and negative cooling field (red symbols)¹⁸, vanishing at T_N . The magnetoresistance $\Delta R/R_0$ of the sample obtained from $\sin^2(\alpha, \beta, \gamma)$ fits to the angle dependent data for all three rotation planes and temperatures are summarized in the lower panel. The Néel temperature is indicated by the orange dashed line. A vanishing MR is observed below T_N for all three rotation configurations. When increasing the temperature, the MR increases until $T \sim 45^\circ\text{C}$ where it seems to saturate.

phase, saturating at a level of $\Delta R/R > 1 \times 10^{-4}$ around $T \sim 45^\circ\text{C}$. A non-vanishing MR above the Curie temperature was inferred by Aqeel *et al.* in bilayers of the ferrimagnetic insulator Cu_2OSeO_3 and Pt via ip rotations only, and attributed to a field induced paramagnetic magnetization acting as sink for the spin accumulation at the Pt interface.²¹ However, the MR discussed by Aqeel *et al.* amounts to about $\Delta R_{\text{trans}} \lesssim 0.07$ m Ω in the paramagnetic phase. Taking the thickness of their platinum film $t_{\text{Pt}} = 5$ nm and a specific resistance of Pt of $\rho \sim 200$ n Ω m, this translates to a magnitude of the MR of $\Delta \rho_{\text{trans}}/\rho \lesssim 2 \times 10^{-6}$. Therefore, the magnetoresistance observed by Aqeel *et al.* is roughly two orders of magnitude smaller than the paramagnetic SMR reported here. Furthermore, no saturation was observed by these authors even at 200 K above the Curie temperature²¹, in contrast to the behavior in our samples evident from Fig. 3. We also would like to stress again that the MR we observe in three orthogonal rotation planes has the symmetry characteristic of SMR, well above T_N .

The saturation value of $(\Delta R/R)_{\text{oopj}} = 1.8 \times 10^{-4}$ we observe here is smaller by roughly a factor of 7 when compared to the best YIG/Pt heterostructures² with comparable platinum thickness. This indicates a good interfacial quality of our heterostructures. Furthermore, in terms of angular momentum sinking capability across

the interface to a metal, Cr_2O_3 in the paramagnetic phase thus still appears to be comparable to a good ferrimagnet. In addition, the SMR signal persists well above T_N , with an apparent saturation or T -independent level in the range $45^\circ\text{C} < T < 60^\circ\text{C}$.

We tentatively attribute the large SMR observed in the paramagnetic phase to a transfer of angular momentum from the Pt onto paramagnetic Cr moments in Cr_2O_3 . However, control experiments in a $\text{Gd}_3\text{Ga}_5\text{O}_{12}/\text{Pt}$ heterostructure with a platinum thickness of 3 nm reveal a vanishing MR, i.e. $\Delta R/R \leq 1 \times 10^{-6}$, around room temperature. Thus, the presence of a finite, magnetic field induced paramagnetic magnetization apparently is not sufficient for the occurrence of a large SMR. In addition, the increase of the SMR magnitude with increasing T even above the ordering temperature is counter-intuitive for a paramagnet.

More quantitatively, the magnetic susceptibility of $\text{Gd}_3\text{Ga}_5\text{O}_{12}$ (GGG) at room temperature is $\chi_{GGG} \approx 6.8 \times 10^{-3}$ according to both a Curie-Weiss susceptibility calculation and experiments.²⁸ In comparison, Foner reported the susceptibility of Cr_2O_3 to be $\chi_{\text{Cr}_2\text{O}_3} \approx 1.6 \times 10^{-3}$ at room temperature²⁹, such that the magnetic field induced magnetization in GGG should be about a factor 4 larger than in Cr_2O_3 in the temperature range of interest here. In spite of this comparable magnetization, the SMR observed in the respective heterostructures of Cr_2O_3 and $\text{Gd}_3\text{Ga}_5\text{O}_{12}$ with Pt differs by more than 2 orders of magnitude. This could be due to the fact that the magnetic moments in GGG are the $4f$ moments of Gd, which are strongly localized and thus might not couple well to the spin accumulation in Pt. In other words, the effective mixing conductance in GGG/Pt could be much smaller than in $\text{Cr}_2\text{O}_3/\text{Pt}$, since for the latter the coupling is mediated by the $3d$ moments on Cr. This would be consistent with the observations by Aqeel *et al.* for $\text{Cu}_2\text{OSeO}_3/\text{Pt}$, where $3d$ moments are responsible for the magnetism. However, more comprehensive SMR experiments in different paramagnetic insulator/Pt heterostructures will be needed in the future to fully clarify the microscopic nature of the paramagnetic SMR effect.

In summary, we measured the magnetoresistive response in $\text{Cr}_2\text{O}_3/\text{Pt}$ heterostructures for different temperatures close to the Néel temperature. Comparing the MR in three mutually orthogonal rotation planes, we find a signal consistent with a positive SMR with a magnitude $\lesssim 2 \times 10^{-4}$ several 10 K above the Néel temperature, which we attribute to a field-induced paramagnetic magnetization in the Cr_2O_3 . Furthermore, our experiments reveal that the mechanism leading to a finite SMR in the paramagnetic phase can not be attributed solely to the field induced magnetization, as no SMR was observed in GGG/Pt heterostructures, hinting at the microscopic mechanisms involved in the SMR. Upon crossing the Néel temperature into the antiferromagnetic phase of Cr_2O_3 , the SMR signal decreases by more than one order of magnitude. Thus, the SMR can be used to probe the mag-

netic phase transition of the AFM in thin film AFMI/Pt microstructures.

We thank H. Gomonay, J. Barker and U. K. Rößler for fruitful discussions as well as M. Lammel and S. Piontek for technical support. We acknowledge financial support by the Deutsche Forschungsgemeinschaft via SPP 1538 (project no. GO 944/4 and TH 1399/5).

- ¹Y.-T. Chen, S. Takahashi, H. Nakayama, M. Althammer, S. T. B. Goennenwein, E. Saitoh, and G. E. W. Bauer, *Physical Review B* **87**, 144411 (2013).
- ²M. Althammer, S. Meyer, H. Nakayama, M. Schreier, S. Altmannshofer, M. Weiler, H. Huebl, S. Geprägs, M. Opel, R. Gross, D. Meier, C. Klewe, T. Kuschel, J.-M. Schmalhorst, G. Reiss, L. Shen, A. Gupta, Y.-T. Chen, G. E. W. Bauer, E. Saitoh, and S. T. B. Goennenwein, *Physical Review B* **87**, 224401 (2013).
- ³H. Nakayama, M. Althammer, Y.-T. Chen, K. Uchida, Y. Kajiwara, D. Kikuchi, T. Ohtani, S. Geprägs, M. Opel, S. Takahashi, R. Gross, G. E. W. Bauer, S. T. B. Goennenwein, and E. Saitoh, *Physical Review Letters* **110**, 206601 (2013).
- ⁴J. E. Hirsch, *Physical Review Letters* **83**, 1834 (1999).
- ⁵M. Isasa, A. Bedoya-Pinto, S. Vélez, F. Golmar, F. Sánchez, L. E. Hueso, J. Fontcuberta, and F. Casanova, *Applied Physics Letters* **105**, 142402 (2014).
- ⁶K. Ganzhorn, J. Barker, R. Schlitz, B. A. Piot, K. Ollefs, F. Guillou, F. Wilhelm, A. Rogalev, M. Opel, M. Althammer, S. Geprägs, H. Huebl, R. Gross, G. E. W. Bauer, and S. T. B. Goennenwein, *Physical Review B* **94**, 094401 (2016).
- ⁷A. Aqeel, N. Vlietstra, A. Roy, M. Mostovoy, B. J. van Wees, and T. T. M. Palstra, *Physical Review B* **94**, 134418 (2016).
- ⁸E. V. Gomonay and V. M. Loktev, *Low Temperature Physics* **40**, 17 (2014).
- ⁹P. Wadley, B. Howells, J. Železný, C. Andrews, V. Hills, R. P. Campion, V. Novák, K. Olejník, F. Maccherozzi, S. S. Dhesi, S. Y. Martin, T. Wagner, J. Wunderlich, F. Freimuth, Y. Mokrousov, J. Kuneš, J. S. Chauhan, M. J. Grzybowski, A. W. Rushforth, K. W. Edmonds, B. L. Gallagher, and T. Jungwirth, *Science* **351**, 587 (2016).
- ¹⁰X. Marti, I. Fina, C. Frontera, J. Liu, P. Wadley, Q. He, R. J. Paull, J. D. Clarkson, J. Kudrnovský, I. Turek, J. Kuneš, D. Yi, J.-H. Chu, C. T. Nelson, L. You, E. Arenholz, S. Salahuddin, J. Fontcuberta, T. Jungwirth, and R. Ramesh, *Nature Materials* **13**, 367 (2014).
- ¹¹T. Jungwirth, X. Marti, P. Wadley, and J. Wunderlich, *Nature Nanotechnology* **11**, 231 (2016).
- ¹²J. Železný, H. Gao, K. Výborný, J. Zemen, J. Mašek, A. Manchon, J. Wunderlich, J. Sinova, and T. Jungwirth, *Physical Review Letters* **113**, 157201 (2014).
- ¹³H. Wang, D. Hou, Z. Qiu, T. Kikkawa, E. Saitoh, and X. Jin, *Journal of Applied Physics* **122**, 083907 (2017).
- ¹⁴G. R. Hoogeboom, A. Aqeel, T. Kuschel, T. T. M. Palstra, and B. J. van Wees, *Applied Physics Letters* **111**, 052409 (2017).
- ¹⁵J. Fischer, O. Gomonay, R. Schlitz, K. Ganzhorn, N. Vlietstra, M. Althammer, H. Huebl, M. Opel, R. Gross, S. T. B. Goennenwein, and S. Geprägs, arXiv:1709.04158 (2017).
- ¹⁶L. Baldrati, A. Ross, T. Niizeki, R. Ramos, J. Cramer, O. Gomonay, E. Saitoh, J. Sinova, and M. Kläui, arXiv:1709.00910 (2017).
- ¹⁷Y. Ji, J. Miao, K. K. Meng, Z. Y. Ren, B. W. Dong, X. G. Xu, Y. Wu, and Y. Jiang, *Applied Physics Letters* **110**, 262401 (2017).
- ¹⁸T. Kosub, M. Kopte, F. Radu, O. G. Schmidt, and D. Makarov, *Physical Review Letters* **115**, 097201 (2015).
- ¹⁹T. Kosub, M. Kopte, R. Hühne, P. Appel, B. Shields, P. Maletinsky, R. Hübner, M. O. Liedke, J. Fassbender, O. G. Schmidt, and D. Makarov, *Nature Communications* **8**, 13985 (2017).
- ²⁰X. He, Y. Wang, N. Wu, A. N. Caruso, E. Vescovo, K. D. Be-

- lashchenko, P. A. Dowben, and C. Binek, *Nature Materials* **9**, 579 (2010).
- ²¹A. Aqeel, N. Vlietstra, J. A. Heuver, G. E. W. Bauer, B. Noheda, B. J. van Wees, and T. T. M. Palstra, *Physical Review B* **92**, 224410 (2015).
- ²²K. D. Belashchenko, *Physical Review Letters* **105**, 147204 (2010).
- ²³N. Wu, X. He, A. L. Wysocki, U. Lanke, T. Komesu, K. D. Belashchenko, C. Binek, and P. A. Dowben, *Physical Review Letters* **106**, 087202 (2011).
- ²⁴T. Kosub, *Ferromagnet-Free Magnetoelectric Thin Film Elements*, Ph.D. thesis, Technische Universität Chemnitz (2016).
- ²⁵K. Halbach, *Nuclear Instruments and Methods* **169**, 1 (1980).
- ²⁶S. T. B. Goennenwein, R. Schlitz, M. Pernpeintner, K. Ganzhorn, M. Althammer, R. Gross, and H. Huebl, *Applied Physics Letters* **107**, 172405 (2015).
- ²⁷W. Limmer, M. Glunk, J. Daeubler, T. Hummel, W. Schoch, R. Sauer, C. Bihler, H. Huebl, M. S. Brandt, and S. T. B. Goennenwein, *Physical Review B* **74**, 205205 (2006).
- ²⁸Y. J. Kim, C.-Y. Liu, S. K. Lamoreaux, G. Visser, B. Kunkler, A. N. Matlashov, J. C. Long, and T. G. Reddy, *Physical Review D* **91**, 102004 (2015).
- ²⁹S. Foner, *Physical Review* **130**, 183 (1963).